Jurnal Elektronika dan Telekomunikasi (JET), Vol. 25, No. 2, December 2025, pp. 141-147
Accredited by RISTEKDIKTI, Decree No: **158/E/KPT/2021**
doi: 10.55981/jet.781

Comparative Analysis and Mitigation of Extremely Low Frequency (ELF) Magnetic Field Exposure from Smartphone Internal

Bayu Wira Yudha, Hasballah Zakaria*

School of Electrical Engineering and Informatics
Institut Teknologi Bandung
Jl. Ganesa No.10
Bandung, Indonesia

Abstract

While public concern regarding smartphone electromagnetic field (EMF) exposure is largely focused on radio frequency (RF) emissions, this study investigates the overlooked extremely low frequency (ELF) magnetic fields originating from internal hardware circuits, such as the Power Management Integrated Circuit (PMIC). This research employs a quantitative experimental methodology to characterize and compare the near-field emissions of two smartphone models with distinct internal architectures: the Xiaomi Redmi Note 8 Pro (12nm mid-range chipset) and the Samsung Galaxy S23 (4nm premium chipset). Magnetic field intensity measurements were conducted using a Hall-effect Gaussmeter, both in free space and with a 3D-printed cubic head phantom fabricated from PETG and filled with a conductive saline-based tissue-simulating liquid (TSL). The primary findings reveal unique ELF emission "fingerprints," where the premium-engineered device exhibits a peak exposure of 0.269 mT—nearly three times lower than its mid-range counterpart at 0.799 mT. Theoretical analysis utilizing the Biot-Savart Law attributes this reduction to the minimized current loop areas inherent in advanced 4nm process nodes compared to older 12nm architectures. Quantitative analysis of mitigation strategies demonstrates that spatial separation (a 15 cm distance) is the most dominant factor, achieving up to 90.7% attenuation, which surpasses the material shielding provided by the phantom (82.0%). Although peak contact exposure can exceed the ICNIRP reference level, the rapid near-field decay ensures compliance at minimal practical distances. This study concludes that ELF exposure is a function of engineering quality rather than network technology, and mitigation is most effectively achieved through physical distance.

Keywords: electromagnetic fields (EMF), extremely low frequency (ELF), exposure mitigation, 3D printed phantom, smartphone design, electromagnetic compatibility (EMC).

I. INTRODUCTION

The exponential increase in smartphone adoption has raised significant concerns among the public and the scientific community regarding the potential health impacts of electromagnetic field (EMF) exposure. The majority of public attention and regulatory standards, such as the Specific Absorption Rate (SAR), have concentrated on radio frequency (RF) emissions, originating from the device's communication antennas. These standards are designed to protect against established thermal effects, specifically the heating of biological tissue resulting from the absorption of RF energy. The scientific debate concerning long-term health effects remains ongoing. Some observational and animal studies have suggested a possible link between EMF exposure and various health conditions, including an increased incidence of tumors in laboratory animals after prolonged exposure[1]. Conversely, large-scale prospective cohort studies, such as COSMOS (Cohort Study of Mobile Phone Use and Health), have not yet found a significant increase in brain tumor risk among heavy mobile phone users [2]. The complexity of this scientific evidence underscores the importance of continued research.

This study, however, shifts focus to a frequently neglected yet critical area: magnetic field emissions in the extremely low-frequency (ELF) spectrum. Unlike RF emission, which is intentionally radiated into the far field, ELF emission is an inevitable byproduct of the device's internal circuitry. The primary sources include components with high and fluctuating electrical currents, such as the Power Management Integrated Circuit (PMIC), battery systems, and display circuits [3], [4]. This emission is reactive and dominates the near-field region—the area of direct contact with the user's body—where its intensity can be substantial.

The previous study has confirmed the existence of ELF fields from phone hardware [3]. However, its findings remained largely descriptive and did not investigate how specific internal hardware architectures or advancements in semiconductor process nodes influence emission intensities. Conversely, this study advances the field by directly comparing devices from different market segments and linking the observed emission differences to the quality of engineering design and Electromagnetic Compatibility (EMC) principles—representing a unique contribution of this work.

* Corresponding Author.
Email: hasballah@stei.itb.ac.id
Received: Agustus 14, 2025 ; Revised: November 3, 2025
Accepted: December 9, 2025 ; Published: December 31, 2025

When non-ionizing electromagnetic waves, such as RF and ELF, penetrate biological tissue, their primary interaction is the induction of electric currents. A time-varying electric field (E) causes dielectric polarization and current flow, while a time-varying magnetic field (B) induces eddy currents according to Faraday's Law. For ELF fields, the dominant mechanism is current induction, which can stimulate nerve and muscle tissue if the intensity is sufficiently high [5]. The ELF magnetic field emissions from internal circuits, particularly the power delivery network (PDN), are fundamentally generated by current loops. According to the Biot-Savart law, the strength of the resulting magnetic field is directly proportional to the current's magnitude and the area of the loop. Consequently, effective EMC design practices aim to minimize these current loop areas to reduce unwanted electromagnetic interference (EMI) [2], [6]. Modern Printed Circuit Board (PCB) designs in premium devices often utilize multi-layered architectures with adjacent power and ground planes. This compact and integrated layout inherently reduces current loop areas, physically resulting in lower ELF near-field emissions. In contrast, mid-range devices may employ simpler PCB designs with less optimized component layouts. The choices of device's chassis material further play a role; a conductive metal frame can provide additional passive shielding via the induction of eddy currents, a mechanism absent in non-conductive plastic frames [7].

Safety standards for EMF exposure are frequency-dependent due to differing interaction mechanisms. For the ELF spectrum, the relevant standard is the ICNIRP (International Commission on Non-Ionizing Radiation Protection) guideline for low-frequency fields. The ICNIRP (2010) guidelines establish a reference level for public exposure to magnetic fields from power-frequency sources (50/60 Hz) at 200 μT, or 0.2 mT [5]. This level is intended to prevent nerve stimulation. It is crucial to note that this reference level is derived for uniform, whole-body exposure scenarios. ICNIRP states that for highly localized sources close to the body, a direct comparison may not be appropriate, and internal dosimetry analysis is preferable for an accurate compliance assessment [5].

A critical and novel aspect of this research is the investigation of how semiconductor manufacturing processes influence these emissions. We hypothesize that the transition from older 12nm process nodes to advanced 4nm nodes correlates with reduced ELF emissions. According to the Biot-Savart law, the strength of the magnetic field generated by internal circuits is directly proportional to the current loop area on the PCB. As highlighted in a recent review of EMI challenges, modern power electronic architectures increasingly employ tighter integration techniques that theoretically minimize these loop areas, thereby improving the EMC[8].

Furthermore, this study addresses the methodological debate regarding the use of saline phantoms. While critics argue that saline does not replicate the permittivity of brain tissue at RF frequencies, we contend that for ELF magnetic fields, the dominant interaction mechanism is the induction of eddy currents, which is governed by conductivity rather than permittivity. This approach demonstrated that in phantom shell designs, material choices must align with the specific frequency-dependent interaction mechanism. Moreover, recent characterizations confirm that for low-frequency bio-impedance measurements, preserving conductivity matching is the critical parameter for validity [9].

This study addresses this research gap with two primary objectives. First, it quantitatively characterizes and compares the ELF emission "fingerprints" of two smartphone models representing different market segments and engineering philosophies: the Xiaomi Redmi Note 8 Pro (a 4G mid-range device) and the Samsung Galaxy S23 (a 5G premium device). The hypothesis is that the level of ELF emission is more reflective of the internal hardware's engineering quality and EMC than its network generation. Second, this research aims to empirically compare the effectiveness of two fundamental exposure mitigation strategies: material-based shielding, represented by a simple head phantom, and spatial separation. Accordingly, this study not only provides novel exposure data but also offers practical insights into the hardware design factors influencing ELF exposure and the most effective methods for its mitigation [10], [11].

II. METHODS

This research implemented a quantitative experimental approach to measure and analyze the magnetic field (B-field) intensity from smartphones under controlled conditions.

A. Design and Devices for Experiments

Two smartphone models were selected to represent different hardware architectures: the Xiaomi Redmi Note 8 Pro, equipped with a MediaTek Helio G90T chipset (built on a 12nm process), and the Samsung Galaxy S23, powered by a Qualcomm Snapdragon 8 Gen 2 for Galaxy chipset (manufactured with a more advanced 4nm process). Magnetic field strength was measured using an F.W. Bell 5100 series Gaussmeter equipped with a transversal Hall-effect probe. This device provides a typical frequency response from DC to 10 kHz, ensuring that it specifically measures magnetic fields in the ELF spectrum generated by internal circuitry, without interference from RF emissions from the antennas.

B. Phantom Fabrication and TSL Preparation

A simplified head phantom system was designed, as depicted in Figure 1, to evaluate the effectiveness of a representative material. Both a CAD model of a cubic phantom with external dimensions of 15 cm x 15 cm x 15 cm and a wall thickness of 5 mm were prepared with the use of Autodesk Fusion 360 software. The phantom shell was then fabricated using Fused Deposition Modeling (FDM) 3D printing technology with Polyethylene Terephthalate Glycol (PETG) filament.

While anatomically correct phantoms, such as the Specific Anthropomorphic Mannequin (SAM), are the standard for SAR testing, a simplified cubic geometry was intentionally selected for this study. This approach

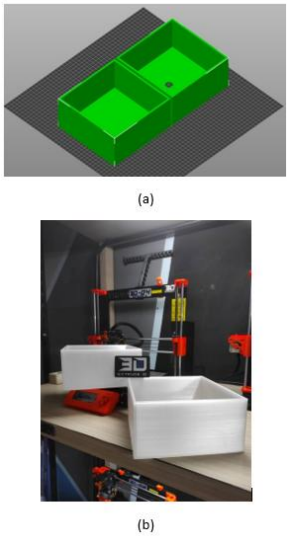

Figure 1 (a) Phantom Design in Autodesk Fusion 360. (b) The 3D-printed Phantom

provides a standardized, repeatable volume for the tissue-simulating liquid or TSL, enabling an unambiguous analysis of the fundamental physical principles of attenuation without the confounding geometric complexities associated with an anatomical model.

The Tissue Simulating Liquid (TSL) employed was a 0.9% w/v saline solution (27g NaCl in 3L deionized water). This solution achieves a conductivity of $\sigma \approx 1.5$ S/m. While its permittivity differs from the complex brain tissue models described in older literature, recent dielectric studies by indicate that age and tissue variations significantly affect permittivity, yet conductivity remains the primary determinant for induced currents in the ELF range [12]. Therefore, aligning with the suggested optimized measurement protocols, the saline solution serves as a valid, worst-case model for evaluating magnetic shielding effectiveness via induced eddy currents [9].

C. Measurement Procedure and Layout

Measurements were conducted across four primary configurations, as illustrated in Figure 2: (a) baseline measurements at close contact (1-2 mm) without the phantom, (b) measurements at a 15 cm distance to quantify spatial attenuation, (c) measurements with the empty PETG phantom to isolate the shell's effect, and (d) measurements with the phantom filled with the saline TSL to evaluate the combined effect. During all measurements, the probe's position and angular orientation were systematically varied (0°, 30°, 45°, 60°, and 90°) to map the field distribution comprehensively. In this case, the probe-to-surface distance was consistently maintained at 1-2 mm to ensure accurate near-field assessment.

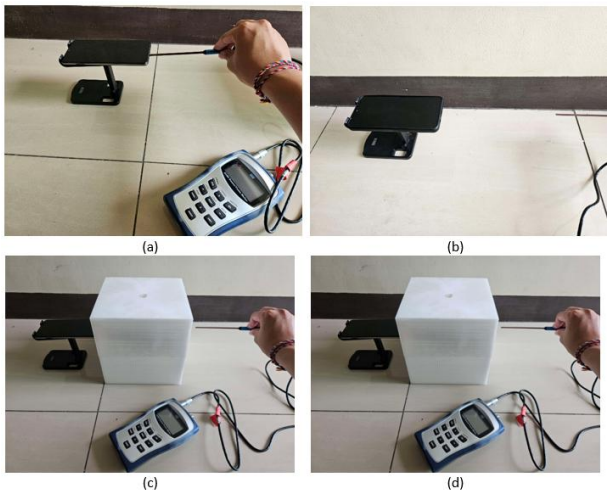

Figure 2. ConceptualSchematic of the Experimental Setup: (a) Without Phantom, (b) Without Phantom at a Distance, (c) With Phantom, (d) With Phantom and TSL Saline.

Each data point reported in the results represents the mean of eight repeated measurements, ensuring (statistical) reliability. The consistently low standard deviation across all measurements indicates a high degree of precision and reproducibility in the experimental procedure. Furthermore, the methodological limitation of the simple saline TSL must be acknowledged: while it accurately mimics the conductivity necessary to study eddy-current-induced magnetic field attenuation, its elevated permittivity differs from that of brain tissue. Accordingly, the study specifically focuses on the magnetic field attenuation mechanism, and its results may not fully replicate the interaction of the total electromagnetic wave with a human head.

D. Data Analysis and Statistical Treatment

For each measurement configuration, eight repeated trials were conducted to ensure the reliability and stability of the results. The values presented in this paper represent the mean of these trials. The consistently low standard deviation observed across all measurements, as detailed in the original dataset, indicates a high degree of precision and reproducibility in the experimental setup. This methodological rigor minimizes the impact of random errors and enhances the validity of the findings.

III. Results and Discussion

This section presents the measurement results and offers an in-depth analysis, integrating data presentation with physical interpretation and its implications for device design and safety standards.

A. Hardware Design Reflected in the ELF Emission "Fingerprint"

Baseline measurements at close contact revealed significant differences in the emission profiles between the two devices. The Xiaomi Redmi Note 8 Pro exhibited a peak magnetic field intensity of 0.799 mT, whereas the Samsung Galaxy S23 registered a substantially lower peak value of 0.269 mT—a nearly threefold difference. The full spatial distribution of these baseline emissions is detailed in Table 1.

This disparity extended beyond magnitude to spatial distribution; the Xiaomi device demonstrated a highly concentrated hotspot in one area (at the center position), whereas the Samsung device displayed more evenly distributed emissions. This difference in emission 'fingerprints' is clearly visualized in Figure 3. The spatial distribution is visualized in the heatmaps of

TABLE 1
BASELINE NEAR-FIELD MAGNETIC FIELD INTENSITY (MT) AT CLOSE CONTACT

Phone Model	Position	Angle	B-Field (mT)
Xiaomi Redmi Note 8 Pro	Center	0°	0.406
		30°	0.278
		45°	0.316
		60°	0.404
		90°	0.799
	Right	0°	0.209
		30°	0.218
		45°	0.290
		60°	0.049
		90°	0.105
	Left	0°	0.410
		30°	0.444
		45°	0.575
		60°	0.366
		90°	0.184
Samsung Galaxy S23	Center	0°	0.183
		30°	0.233
		45°	0.259
		60°	0.221
		90°	0.241
	Right	0°	0.176
		30°	0.223
		45°	0.206
		60°	0.236
		90°	0.268
	Left	0°	0.219
		30°	0.205
		45°	0.221
		60°	0.250
		90°	0.269

Degree (◦)	Center	Right	Left
0	0,406	0,209	0,41
30	0,278	0,218	0,444
45	0,316	0,29	0,575
60	0,404	0,049	0,366
90	0,799	0,105	0,184

(a)

Degree (◦)	Center	Right	Left
0	0,183	0,176	0,219
30	0,233	0,223	0,205
45	0,259	0,206	0,221
60	0,221	0,236	0,25
90	0,241	0,268	0,269

(b)

Figure 3. Heatmap Comparison of ELF Emission 'Fingerprints' (Without Phantom) for (a) Xiaomi Redmi Note 8 Pro and (b) Samsung Galaxy S23. The Color Gradient Represents the B-Field Intensity (mT), Ranging from Green (Minimum) to Red (Maximum Intensity).

Figure 3, providing compelling visual confirmation of the differing emission 'fingerprints.' In Figure 3a, the intense coloration corresponding to the 0.799 mT peak is sharply localized to the center position at a 90° orientation, suggesting a single, dominant emission source within the Xiaomi device's power delivery network. In contrast, Figure 3b reveals a more diffuse pattern of lower-intensity fields across the Samsung device's surface, with no single dominant concentration. This contrasting visual evidence strongly supports the conclusion that the premium device employs a more electromagnetically compatible internal layout.

This difference can be considered a unique ELF emission "fingerprint" for each device, directly reflecting the quality and engineering philosophy of its internal hardware. As previously discussed, ELF magnetic field emissions from the PDN are fundamentally generated by current loops. Effective EMC design aims to minimize these loops to reduce EMI. [2], [6].

This disparity confirms the "Fingerprint Hypothesis." The 4nm architecture of the Samsung device enables a reduction in the physical area of high-current loops within the PMIC and PCB layout. In the investigation of pre-layout EMI estimation, research emphasizes that minimizing the parasitic loop inductance in DC-DC converters is the most effective method for reducing conducted emissions [13]. Our data aligns with recent findings, suggesting that the advanced integration of the 4nm chipset inherently reduces the radiated magnetic field magnitude. Furthermore, the aluminum chassis of the Samsung device likely provides passive shielding by supporting the formation of surface eddy currents, a mechanism absent in the plastic-bodied Xiaomi.

In contrast, the Xiaomi Redmi Note 8 Pro's MediaTek Helio G90T, a mid-range SoC built on an older 12nm process, likely has a less integrated power architecture. This can result in component layouts with larger and less electromagnetically shielded current loops, thereby generating stronger stray magnetic fields.

Furthermore, the device's chassis material also contributes. The conductive "Armor Aluminum" frame of the Samsung S23 can provide an additional passive shielding effect through the induction of eddy currents within the frame itself, a mechanism absent in the non-conductive plastic frame of the Xiaomi [14]. Thus, it is evident that the level of near-field ELF exposure is not a function of network technology generation (4G vs. 5G), but rather a predictable consequence of the quality of electrical design, chipset integration levels, and the EMC principles applied at the hardware level.

B. Quantitative Analysis of Mitigation Strategies: Physical Distance vs. Material Shielding

It is instructive to examine the specific measurement results for each device separately before providing a condensed breakdown of the mitigation strategies. Table 2 presents the Xiaomi Redmi Note 8 Pro's measurement data, which shows a clear and intense emission profile. A notable hotspot was detected at the center position with a 90° probe orientation under baseline conditions without a phantom, recording a peak magnetic field intensity of 0.799 mT.

TABLE 2
ATTENUATION ANALYSIS AT THE HOTSPOT FOR XIAOMI REDMI NOTE 8 PRO

Measurement Condition	Position	Angle	B-Field Intensity (mT)
Baseline (No Phantom)	Center	90°	0.799
With Empty Phantom	Center	90°	0.239
With Saline Phantom	Center	90°	0.144

The field at this hotspot was reduced to 0.239 mT by the introduction of the empty PETG shell alone, which resulted in significant attenuation. The field was further decreased to 0.144 mT when the saline TSL was poured into the phantom. This step-by-step analysis shows that an additional 0.095 mT of attenuation was caused by the saline TSL itself. This decrease is directly related to the liquid's conductive characteristics and the ensuing induction of opposing eddy currents.

The Samsung Galaxy S23, on the other hand, showed a radically different and lower-intensity emission profile, as shown in Table 3. Its peak emission, measured at a 90° orientation on the left, was 0.269 mT, which is almost three times less than the Xiaomi device's peak emission. This peak value was lowered to 0.119 mT by the empty phantom and to 0.109 mT by the full saline-filled phantom. This indicates that the saline TSL only contributed 0.010 mT of additional attenuation. Faraday's law of induction is consistent with this less notable effect; the Samsung device's weaker initial magnetic field caused less significant eddy currents in the conductive liquid, which led to a smaller shielding contribution from the TSL than the Xiaomi device. The context required for the subsequent condensed quantitative analysis is supplied by these individual device results.

Table 4 presents a quantitative decomposition of the attenuation effects at the highest identified hotspot for each device, allowing for a direct comparison of the effectiveness of mitigation strategies.

The data in Table 4 reveal several crucial findings. First, the complete phantom system (PETG shell and saline TSL) proved highly effective at reducing exposure, achieving an attenuation rate of 82.0% for the Xiaomi device. The attenuation mechanism is twofold: minor reflection and absorption by the dielectric PETG shell, and the induction of eddy currents by the conductive saline TSL. According to Lenz's Law, these eddy currents generate a secondary magnetic field that opposes the primary field from the phone, causing further attenuation. Notably, the absolute attenuation provided by the TSL was more pronounced for the Xiaomi device, consistent with Faraday's law of induction, dictating that the strength of the induced eddy currents—and thus the opposing magnetic field they generate—is proportional to the rate of change of the primary magnetic flux. On the other hand, because the Xiaomi device induced more substantial eddy currents in the conductive saline, it resulted in a more significant shielding effect.

However, the most significant finding pertains to the comparison between the phantom's effectiveness and that of physical distance. For the Xiaomi device, maintaining a distance of just 15 cm resulted in an attenuation of 90.7%, surpassing the attenuation achieved by the material-based phantom. This provides compelling quantitative evidence that for ELF magnetic field exposure in the near-field region, spatial separation is the most superior and practical mitigation strategy for users [10], [11]. This finding resonates with the exposimetric comparisons, which suggest that for near-field sources, spatial separation remains the most practical and effective "filter" for user exposure, often outperforming material-based shielding solutions in real-world scenarios [4].

The comparative bar chart in Figure 4 visually illustrates the efficacy of the mitigation strategies. For the Xiaomi device, the reduction from the initial 'Close Contact' bar to the '15 cm Distance' bar (a 90.7% decrease) is markedly larger than the reduction to the 'With Phantom' bar (an 82.0% decrease). This visualization obviously underscores the paper's central finding: for near-field ELF magnetic fields, spatial separation is a more dominant and effective mitigation factor than the introduction of a material-based shield. (or the dominant capacity of spatial separation as an effective mitigation of ELF exposure).

TABLE 3
ATTENUATION ANALYSIS AT THE HOTSPOT FOR SAMSUNG GALAXY S23

Measurement Condition	Position	Angle	B-Field Intensity (mT)
Baseline (No Phantom)	Left	90°	0.269
With Empty Phantom	Left	90°	0.119
With Saline Phantom	Left	90°	0.109

TABLE 4
QUANTITATIVE DECOMPOSITION OF ATTENUATION EFFECTS AT THE HIGHEST HOTSPOT

Parameter	Xiaomi Redmi Note 8 Pro (Center, 90°)	Samsung Galaxy S23 (Left, 90°)
1. Initial Field (Close Contact)	0.799 mT (100%)	0.269 mT (100%)
2. Field with Total Phantom	0.144 mT (18.0%)	0.109 mT (40.5%)
3. Field at 15 cm Distance	0.074 mT (9.3%)	0.111 mT (41.3%)
Total Attenuation by Phantom (1-2)	0.655 mT (82.0% Reduction)	0.160 mT (59.5% Reduction)
Total Attenuation by Distance (1-3)	0.725 mT (90.7% Reduction)	0.158 mT (58.7% Reduction)

C. Validation of Near-Field Characteristics and Implications for Safety Standards

The measurement data at varying distances enable the experimental validation that the observed emissions are near-field in nature. In the far-field region, the field amplitude decays proportionally to 1/r, where r denotes the distance. In contrast, in the near-field region, reactive field components decay much more rapidly, with terms proportional to $1/r^2$ or $1/r^3$. A quantitative

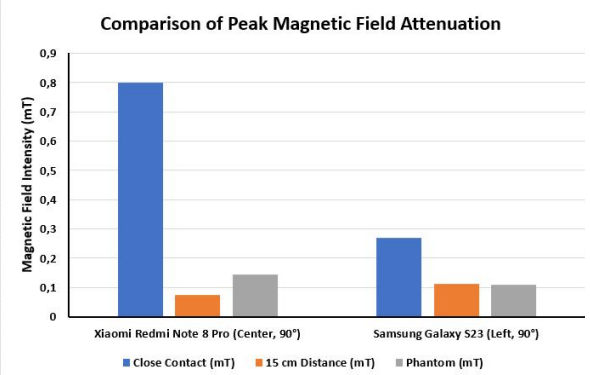

Figure 4. Comparative Analysis of Mitigation Strategies on Peak Magnetic Field Intensity.

analysis of the Xiaomi data reveals a measured decay factor of approximately 10.8 (from 0.799 mT to 0.074 mT over 15 cm). This decay is steeper than predicted by a far-field (1/r) model, thereby providing definitive confirmation of the near-field nature of these emissions.

This rapid decay characteristic has important implications when contextualizing the measurement results against safety standards. As previously mentioned, the relevant standard is the ICNIRP (2010) guideline for ELF, which sets a Reference Level for the general public at 0.2 mT [5].

When compared directly, the intensities of values measured at close proximity for both devices (0.799 mT for Xiaomi and 0.269 mT for Samsung) exceed this reference level. However, a scientifically accurate interpretation must consider two crucial factors. First, the ICNIRP Reference Level is intended for scenarios involving uniform, whole-body exposure and not for highly concentrated, localized exposure from a small source like a smartphone. ICNIRP itself states that for highly localized sources, a direct comparison with the reference level may not be appropriate.

Second, and most importantly, is the rapid decay of the near-field. As the data shows, the field intensity for both devices decrease significantly to below the 0.2 mT reference level at a distance of 15 cm. This indicates that for any practical usage scenario involving even minimal separation (e.g., a phone in a pocket, on a table, or used with a headset), the average exposure level to the body is likely well within the established safety guidelines. These findings highlight the significance of distance as a primary mitigation factor and the importance for careful analysis when applying exposure standards to complex near-field sources.

IV. CONCLUSION

Based on the presented results and analysis, this research establishes that each smartphone generates a unique and quantifiable ELF magnetic field emission "fingerprint," which is directly dependent on the quality of its internal hardware design. Devices with more integrated chipsets and PMIC architectures, coupled with superior EMC principles, exhibit significantly lower emission levels, confirming that ELF exposure is a function of engineering quality rather than simply network technology generation (4G vs. 5G). Furthermore, in a quantitative comparison of mitigation strategies, spatial separation was experimentally proven to be the most dominant and effective mechanism for near-field ELF exposure, with the attenuation achieved by maintaining a minimal 15 cm distance surpassing the effectiveness of material shielding. Finally, although the magnetic field intensity at direct contact can exceed the ICNIRP Reference Level for public exposure, the rapid decay characteristic of the near-field is a crucial intrinsic safety factor. The exposure intensity drops drastically to below the reference level at minimal practical usage distances, underscoring the importance of maintaining distance as the most effective safety practice.

While these findings are robust, the study has certain limitations that define clear directions for future research. The use of a simplified cubic phantom and a saline TSL that only mimics conductivity suggests an opportunity for refinement. Future work should incorporate anatomically correct phantoms and TSLs that replicate both the conductivity and permittivity of brain tissue to enable a more comprehensive dosimetric analysis. Additionally, future investigations should consider more diverse and demanding operational scenarios, such as during active data transfer, gaming, or charging, which may significantly alter the emission profile. A more granular mapping of the field decay at multiple distances is further likely to allow for a more precise mathematical modeling of the near-field profile. Finally, complementing the current measurements with a spectrum analyzer would enable the identification of specific ELF emission frequencies, potentially linking them directly to the switching frequencies of components like the PMIC and providing definitive evidence of their origin.

DECLARATIONS

Conflict of Interest

The authors have declared that no competing interests exist.

Credit Authorship Contribution

Bayu Wira Yudha: Conceptualization, Methodology, Software, Validation, Investigation, Data Curation, Writing Original Draft, Visualization; Hasballah Zakaria: Supervision, Writing, Review & Editing, Project Administration.

Funding

The author(s) received no financial support for the research, authorship, and/or publication of this article.

Acknowledgment

The authors would like to express their gratitude for the assistance provided in preparing the measurement instruments and to colleagues for their constructive discussions and feedback throughout this research.

REFERENCES

[1] L. Falcioni *et al.*, "Report of final results regarding brain and heart tumors in sprague-dawley rats exposed from prenatal life until natural death to mobile phone radiofrequency field representative of a 1.8 ghz gsm base station environmental emission," *Environ. Res.*, vol. 165, no. October 2017, pp. 496–503, 2018, doi: 10.1016/j.envres.2018.01.037.

[2] M. Feychting *et al.*, "Mobile phone use and brain tumour risk – cosmos, a prospective cohort study," *Environ. Int.*, vol. 185, no. January, p. 108552, 2024, doi: 10.1016/j.envint.2024.108552.

[3] J. Misek *et al.*, "Extremely low frequency magnetic fields emitted by cell phones," *Front. Phys.*, vol. 11, no. January, 2023, doi: 10.3389/fphy.2023.1094921.

[4] S. Miclaus, D. B. Deaconescu, D. Vatamanu, and A. M. Buda, "An exposimetric electromagnetic comparison of mobile phone emissions: 5g versus 4g signals analyses by means of statistics and convolutional neural networks classification," *Technologies*, vol. 11, no. 5, 2023, doi: 10.3390/technologies11050113.

[5] International Commission on Non-Ionizing Radiation Protection (ICNIRP), "Guidelines for limiting exposure to electromagnetic fields (100 kHz to 300 GHz)," *Health. Phys.*, vol. 118, no. 5, pp. 483–524, May 2020, doi: 10.1097/HP.0000000000001210.

[6] Y. Akinay, U. Gunes, B. Çolak, and T. Cetin, "Recent progress of electromagnetic wave absorbers: a systematic review and bibliometric approach," *ChemPhysMater*, vol. 2, no. 3, pp. 197–206, 2023, doi: 10.1016/j.chphma.2022.10.002.

[7] C. Ianniello *et al.*, "Synthesized tissue-equivalent dielectric phantoms using salt and polyvinylpyrrolidone solutions," *Magn.*

Reson. Med., vol. 80, no. 1, pp. 413–419, 2018, doi: 10.1002/mrm.27005.

[8] L. Yuan, J. Zhang, Z. Liang, M. Hu, G. Chen, and W. Lu, "EMI challenges in modern power electronic-based converters: Recent advances and mitigation techniques," *Front. Electron*., vol. 4, Nov. 2023, Art. no. 1274258, doi: 10.3389/felec.2023.1274258.

[9] Y. Shi, X. Bai, J. Yang, X. Wu, and L. Wang, "Optimized measurement methods and systems for the dielectric properties of active biological tissues in the 10 Hz–100 MHz frequency range," *Front. Physiol*., vol. 16, Jan. 2025, Art. no. 1537537, doi: 10.3389/fphys.2025.1537537.

[10] A. Peyman, C. Gabriel, and E. H. Grant, "Complex permittivity of sodium chloride solutions at microwave frequencies," *Bioelectromagnetics*, vol. 28, no. 4, pp. 264–274, 2007, doi: 10.1002/bem.20271.

[11] G. Schmid, G. Neubauer, and P. R. Mazal, "Dielectric properties of human brain tissue measured less than 10 h postmortem at frequencies from 800 to 2450 mhz," *Bioelectromagnetics*, vol. 24, no. 6, pp. 423–430, 2003, doi: 10.1002/bem.10123.

[12] S. Marmin *et al.*, "NeuroImage linking dielectric dispersion and age in brain tissues via water content-based electric properties tomography," *Neuroimage*, vol. 322, no. June, p. 121559, 2025, doi: 10.1016/j.neuroimage.2025.121559.

[13] E. Y. Shchuchkin, "Pre-layout DC–DC converter conductive EMI level estimation," *AIP Conf. Proc.,* Dec. 2022, doi: 10.1063/5.0128374.

[14] B. J. Lee, R. D. Watkins, C. M. Chang, and C. S. Levin, "Low eddy current rf shielding enclosure designs for 3t mr applications," *Magn. Reson. Med.*, vol. 79, no. 3, pp. 1745–1752, 2018, doi: 10.1002/mrm.26766.